Design and Implementation of a Perfect Optical Vortex Sorter Using a Binary Dammann Grating

Redha H. Al Ibrahim, Shuiqin Zheng, Tien Khee Ng, *Senior Member, IEEE*, and Boon S. Ooi, *Fellow, IEEE*

***Abstract*—This paper presents the design, simulation, and experimental validation of a Perfect Optical Vortex (POV) sorter using a novel approach based on a binary Dammann Grating. POV beams, crucial for applications in communication and quantum systems, have traditionally posed challenges in sorting due to crosstalk and fabrication limitations. In this study, a hybrid lens system, combining a modified radial lens and a lateral lens, was proposed and optimized using parameters α and β to achieve precise separation between POV modes. The design was simulated, allowing for the customization of the lens based on beam size and system constraints. To further enhance sorting efficiency, a Dammann Grating was employed to encode the phase profile, facilitating easy fabrication and integration into existing optical setups. Simulations and experiments were conducted, demonstrating the system's ability to map each topological charge to a unique radial location with high efficiency. Results indicated minimal crosstalk when the separation between orders exceeded 3, showcasing the potential for this system to be utilized in communication platforms. This research introduces a scalable, efficient, and compact solution for demultiplexing POV beams, paving the way for their seamless integration into optical communication systems.**

***Index Terms*—Binary Dammann grating, orbital angular momentum, perfect optical vortex, spatial division multiplexing, hybrid lens system.**

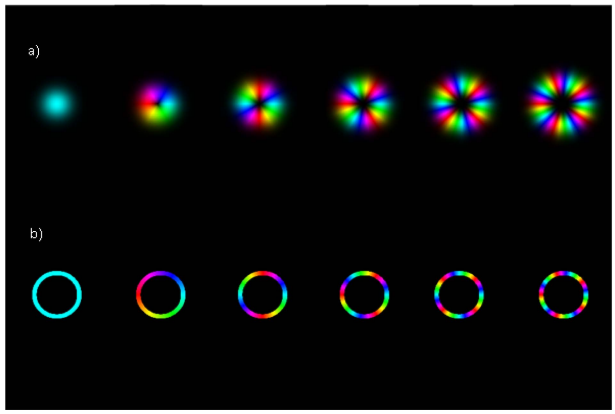

Fig. 1. (a) Simulation of OAM modes using Laguerre-Gaussian beam OAM 0 – 5. (b) simulation of POV with charge 0-5.

I. Introduction

ORBITAL angular momentum (OAM) carrying beams have been extensively investigated in recent years due to their promising impact on various applications, particularly in communication and quantum technologies [1], [2]. One specific category of OAM beams, known as Perfect Optical Vortex (POV) beams, has attracted attention for their potential in realizing spatial division multiplexing systems in both free-space and optical fiber channels [3], [4]. POV beams are characterized by their ring-shaped intensity distribution and their orbital angular momentum carrying phase $e^{il\theta}$, where θ represents the azimuthal angle to the propagation axis, and l is the topological charge [1], [2], [3], [4]. These OAM carrying beams are orthogonal in l, making them suitable for spatial division multiplexing systems [1], [2], [3], [4]. POV beams differ from regular OAM beams in that their ring profile is independent of the topological charge, making them suitable for optical channels as the optical elements remain constant regardless of the topological charge [5].

In recent years, efficient generation of POV beams has been demonstrated using Bessel-Gauss beams and Fourier lenses [3], [4], [6], simulated in Fig. 1(b) and used throughout this work. The generation of POV beams can be achieved using various optical elements, with spatial light modulators (SLM) being one of the most commonly used devices [1], [2], [3], [4], [5], [6], [7]. However, for POV beams to find applications in communication systems, it is essential for detection systems to have the ability to isolate the OAM modes, as each mode serves as an independent channel [8], [9]. Detection of the topological charge thus becomes of utmost importance [9].

Traditionally, the interference of the POV beam with a spherical wavefront has been the method of measuring the topological charge carried by the beam [8], [9]. However, the sensitivity, precision, and specialized optical elements used in optical interferometers render them unsuitable for conventional communication systems [10], [11]. Digital mode sorting is one way to realize

Manuscript received 10 November 2023; revised 29 December 2023; accepted 8 January 2024. Date of publication 16 January 2024; date of current version 30 January 2024. This work was supported in part by the King Abdullah University of Science and Technology Research Funding (KRF) under Grant ORA-2022-5313, and in part by KAUST baseline under Grant BAS/1/1614-01-01, in part by the Great Bay University Scientific Research Start-up Funding under Grant YJKY220005, and in part by the Guangdong Basic and Applied Basic Research Foundation under Grant 2022A1515110496. *(Redha H. Al Ibrahim and Shuiqin Zheng contributed equally to this work.) (Corresponding authors: Shuiqin Zheng; Boon S. Ooi.)*

Redha H. Al Ibrahim, Tien Khee Ng, and Boon S. Ooi are with the Photonics Laboratory, Electrical and Computer Engineering, Division of Computer, Electrical and Mathematical Sciences and Engineering (CEMSE), King Abdullah University of Science and Technology (KAUST), Thuwal 23955-6900, Saudi Arabia (e-mail: boon.ooi@kaust.edu.sa).

Shuiqin Zheng is with the Full-stack Photonics Laboratory, School of Physical Sciences, Great Bay University, Dongguan 523000, China (e-mail: shuiqin.zheng@gbu.edu.cn).

Digital Object Identifier 10.1109/JPHOT.2024.3354279

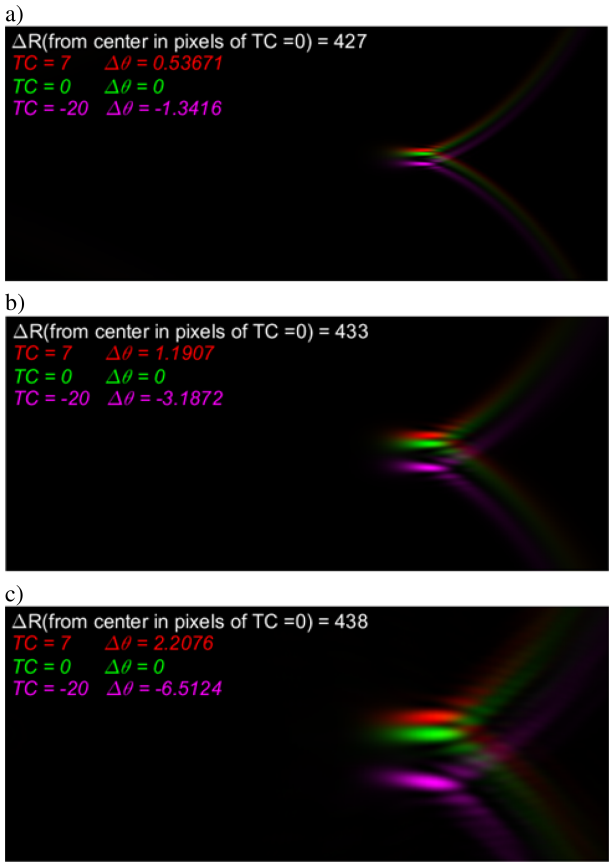

Fig. 2. Output of modified radial lens with different charges inputs. (a) lens with f = 75 mm. (b) lens with f = 175 mm. (c) lens with f = 350 mm. ΔR is the distance from the center of the image to the maximum intensity location of the beam. $\Delta\theta$ is the angular separation between the maximum locations.

optical mode sorting, which is based on the digital processing of the beam [12], [13]. Other methods based on optical modal decomposition have been explored for POV detection, offering lower precision requirements and reduced distortions [14], [15], [16].

Recent developments have shown that Angular lenses can focus the POV beam into radial components that depend on their topological charge [17]. Angular lenses with varying phases have been optimized and utilized for POV sorting based on the topological charge [18]. Some approaches rely on Metasurfaces, while others utilize complex Hybrid lenses, combinations of lens systems such as radial and angular lenses, to improve the separation angle between the modes [19], [20], [21], [22]. However, Metasurfaces pose challenges as demultiplexing platforms due to their polarization dependency, potentially causing issues with higher-order modes having right-hand polarization landing on the same location as low-order modes with left-hand polarization. Additionally, in free-space optical links with beam diameters in centimeters, Metasurfaces are not easily scalable, and their fabrication depends on techniques such as E-Beam Lithography, which are not scalable, expensive, and time-consuming [23].

Hybrid and Angular lenses, although challenging to fabricate due to their non-uniform curvature, can be projected on SLM or phase plates. However, their real-world applications are limited to controlled environments like laboratories and small spaces, as they cannot be easily scaled and require active components [24].

The integration of an angular lens in the sorting process of Perfect Optical Vortex (POV) beams is crucial for its applicability and efficiency. Unlike traditional OAM beams, POV beams maintain a constant ring-shaped intensity distribution irrespective of their topological charge, making them particularly suitable for optical channels. The unique characteristics of POV beams pose challenges in sorting, especially in conventional communication systems where each mode acts as an independent channel. Angular lenses, designed to manipulate the angular components of light, provide an elegant solution for demultiplexing POV beams. By leveraging the distinctive properties of POV beams, such as their radial symmetry and constant ring size, angular lenses can precisely focus and separate different topological charge components. The integration of an angular lens not only ensures accurate sorting but also enhances the overall efficiency of POV-based communication systems, making them more viable for practical applications. This work introduces a system designed employing a Dammann Grating, a binary and easily fabricated structure. The system is scalable and serves as a platform for encoding a phase that represents a superposition of radial and angular lenses. This encoding enables the mapping of each topological charge to a distinct angular location, achieved through a single optical element. The proposed system is not only easy to fabricate but can also be seamlessly integrated into existing Wavelength Division Multiplexing systems. Detailed information on the design and explanation of the damming grating can be found in our prior work, reference [25].

II. Principle and Simulations

For a plane wave expressed in a transverse coordinate system with phase profile e^{ikr}, a converging lens with a transformation function $T(r) = \exp(-i\frac{k}{2f}r^2)$ can separate the different transverse components into unique lateral locations depending on its wave vector k [26].

For a Perfect Optical Vortex (POV) beam, the phase profile is expressed in a cylindrical coordinate system using $e^{il\theta}$. It has been shown in [17], [25] that an axicon phase combined with a quadratic dependence on θ (radial lens) can separate the angular components into unique angular locations. Taking this hint, we modified the phase to be a combination of a transverse lens with a modified radial lens. The modification on the radial lens proposed here is that the phase is defined on an arc dictated by $R\theta$. Thus, the quadratic dependence for the radial lens is in the form of $(\frac{k}{2f}(R_o\theta)^2)$.

Fig. 2 shows the output simulation of the modified radial lens at varying focal lengths and different topological charge inputs. The simulations are carried out using an input beam radius of 1 mm and a ring width of 0.25 mm to support the long focal length in the simulations. It is clear from the output that longer focal lengths require a larger field of view, as the angular separation and radial distance increase with the increase in the

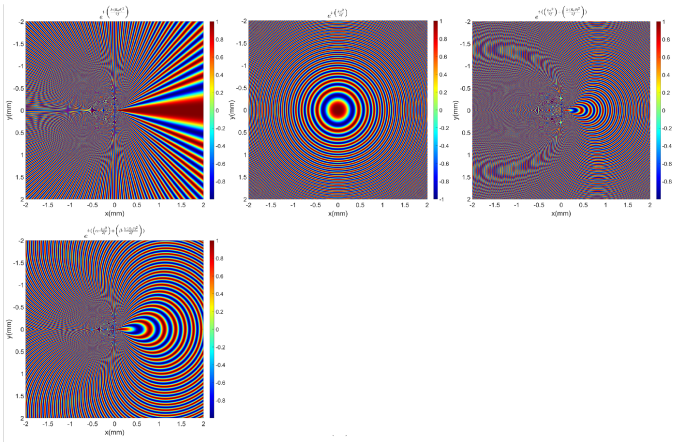

Fig. 3. Full Phase distributions.

focal length of the lens. This poses a challenge for designing the lens for fixed and existing systems, as the lens comes with its own restrictions.

To overcome these restrictions, the radial lens phase is combined with a transverse lens, creating a new hybrid lens with more degrees of freedom and varying strength in the different components of the beam. The hybrid lens allows the system to be tuned and tailored for specific spatial requirements while maintaining compactness. To optimize the phase profile, we start by the superposition of two lenses:

$$\text{Transverse lens} = \frac{k}{2f} r^2 \tag{1}$$

$$\text{Modified radial lens} = \frac{k}{2f} (R_o \theta)^2 \tag{2}$$

$$k = \frac{2\pi}{\lambda} \tag{3}$$

where f is the focal lenght and R_o is the radius of the ring.

$$\text{Phase} = \frac{k}{2f} r^2 + \frac{k}{2f} (R_o \theta)^2 \tag{4}$$

To further optimize this system the strength of each lens can vary, using constants α and β which are used to change the longitudinal and angular strength of the lens, allowing control of the separation between the modes at a focal distance away and thus controlling the number of modes that the system can sort. α and β can be optimized for the input beam size and the focal length of the system as constraints.

$$\text{Optimized hybrid phase} = \frac{k}{2f} \left(\alpha r^2 + \beta (R_o \theta)^2 \right) \tag{5}$$

Fig. 3 shows the phase profiles of each lens and the optimized hybrid lens. To increase computation speed and reduce fabrication time, the final phase profile can be truncated to the beam size and width. Fig. 4 shows the output of the hybrid lens with varying parameters α and β. It is clear from the simulation that varying these parameters can change the separation efficiency, radial location, and angular separation between the modes.

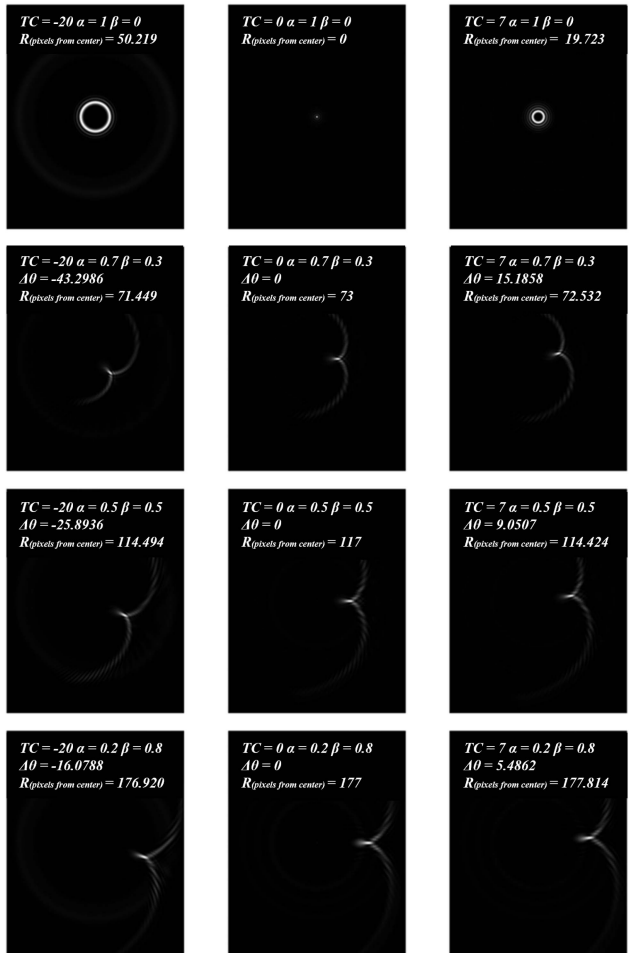

Fig. 4. Output of hybrid lens with varying α and β parameters. f = 175 mm.

Simulations are carried out by varying α and β while constraining the beam size and the focal length to identify the parameters that would best match our system and achieve a separation of about 1° between the center of each mode. $\alpha = 0.35$ and $\beta = 0.65$ have a separation of about 1° for an input beam of radius about 1 mm and width 0.25 mm using $\lambda = 632.8$ nm with a focal length of 175 mm, which is our experimental setup. The phase is then encoded with a 1x2 Dammann grating where the +1-diffraction order carries out the right phase shift [25]. Fig. 5 shows the optimized phase distribution, superimposed on a 1x2 grating distribution, converted to binary, shifted using Dammann Grating transition points, and truncated to match the input beam size. Simulations are carried out using single input (Fig. 6) and multiple inputs (Fig. 7) to verify the design.

To estimate the crosstalk between modes, simulations are carried out with topological charges ranging from -40 to 40. Each simulation includes 21 orders with different steps between the topological charges. The simulations are organized into four sets: the first set with $l = n$, the second set with $l = 2n$, the third set with $l = 3n$, and the fourth set with $l = 4n$, where n is an integer ranging from -10 to 10. Table I shows the output of these simulations, their angular location, and crosstalk.

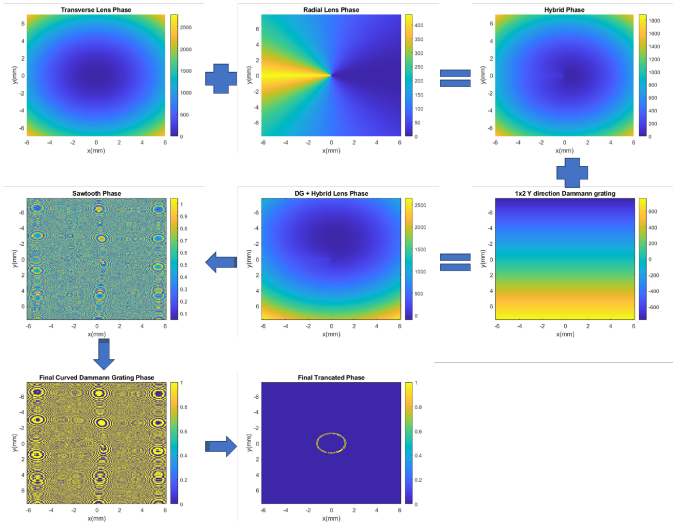

Fig. 5. Optimized phase encoded on 1x2 grating and converted to binary. Truncated to match beam size.

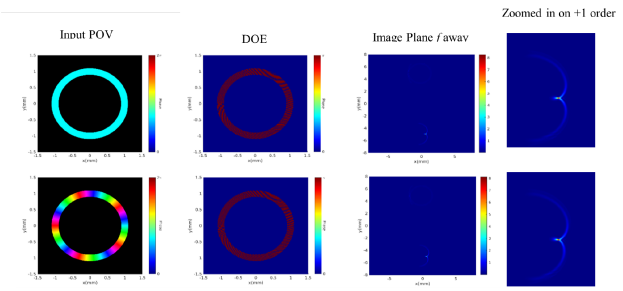

Fig. 6. Single POV input and sorted: (a) POV charge = 0, and (b) POV charge = 5.

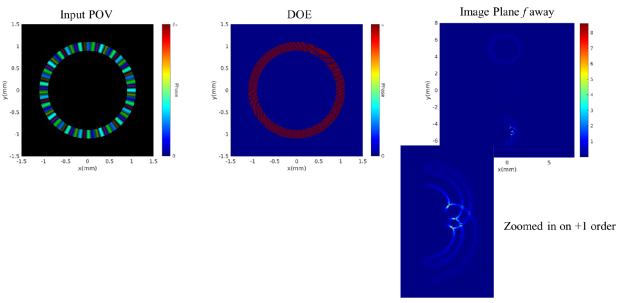

Fig. 7. Multiple POV inputs with POV charge of −35, 0, 40.

The simulations demonstrate that the system can efficiently map each topological charge to a radial location using a single-order input. Howevethe, crosstalk, defined here as the overlap between pixels carrying more than 30% of the incident energy for each mapped mode, is relatively high for practical use in a communication system. Introducing n-steps between orders significantly reduces this overlap. To further minimize it and achieve virtually no overlap, the topological charge $l = 4n$ can be utilized, ensuring non-overlapping mapping of each mode. It's important to note that the center locations of the mapped

TABLE I
OUTPUT OF SIMULATIONS WITH DIFFERENT TOPOLOGICAL CHARGE SETS, THEIR ANGULAR LOCATIONS, AND CROSSTALK

Set	Angular Location vs Order	Crosstalk
$TC = -10:1:10$	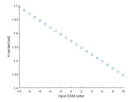	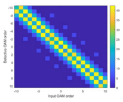
$TC = -20:2:20$	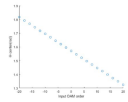	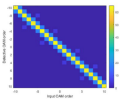
$TC = -30:3:30$	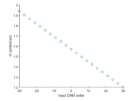	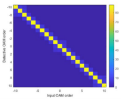
$TC = -40:4:40$	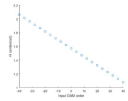	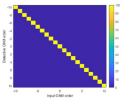

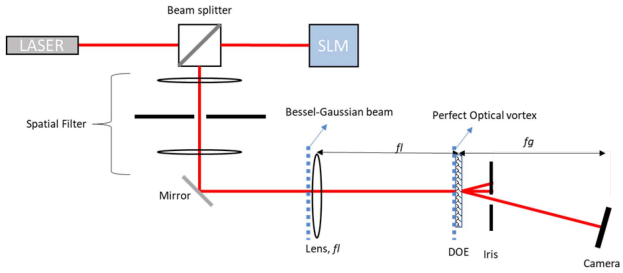

Fig. 8. Illustration of experimental setup.

orders do not overlap in any way. This characteristic opens the possibility of utilizing machine learning algorithms to distinguish between orders, even in scenarios with high crosstalk [27].

III. FABRICATION AND EXPERIMENT

The simulated binary grating is fabricated onto a glass substrate. The designed pattern is transferred into a photoresist-coated glass using a Direct Laser Writer. The pattern is then etched into the glass using Reactive Ion Etching; subsequently, the photoresist is removed, and the device becomes functional [25]. The etching depth h depends on the operating phase shift $\delta\phi$, wavelength λ, and the refractive index of the substrate n following the equation:

$$h = \frac{\lambda\delta\phi}{2\pi(n-1)}$$

The Perfect Optical Vortex (POV) beams are generated using a Spatial Light Modulator (SLM) to generate Bessel-Gaussian beams with topological charge l and a lens to perform a Fourier transformation of the Bessel-Gaussian beam [6], [7]. At the focal plane of the lens, the POV can be observed. The POV sorter is then placed at the focal plane where the POV is generated, and a camera is placed f-away from the sorter, capturing the +1 diffraction order. Fig. 8 shows a schematic of the optical setup.

The experiment is carried out using the same parameters as the simulation, and the results are in good agreement. However,

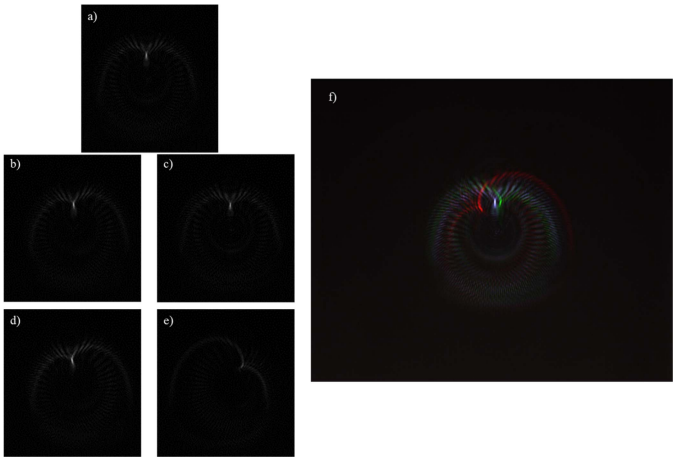

Fig. 9. Experimental results of the sorted POV beams: a) order zero, b) -10, c) +1, d) -5, e) +30. f) shows the overlaped sorted POVs; red represents charge -35, white represents charge 0, and green represents charge 9.

TABLE II
OUTPUT OF SIMULATIONS WITH DIFFERENT TOPOLOGICAL CHARGE SETS, THEIR ANGULAR LOCATIONS, AND CROSSTALK

Set	Angular Location vs Order	Crosstalk
$TC = -10:1:10$	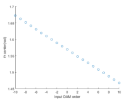	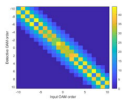
$TC = -20:2:20$	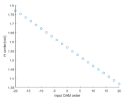	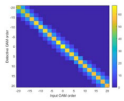
$TC = -30:3:30$	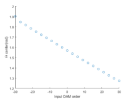	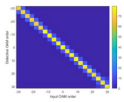
$TC = -40:4:40$	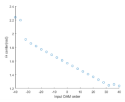	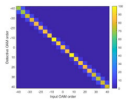

due to stray light, fabrication errors, and alignment errors, the crosstalk in the system is slightly higher, and the sorted angles are slightly shifted. Nevertheless, the system sorted the POV beams with high efficiency. Fig. 9 shows the experimental outputs of some of the modes. Table II presents the experimental outputs, angular separation, and crosstalk for varying topological charges and steps between them, similar to the simulations.

As observed in Fig. 9 and Table II, POV beams can be sorted into locations that correspond to their topological charge, allowing the system to demultiplex an incoming POV using a single passive optical element. Similar to the simulation results, the crosstalk between consecutive orders is high; however, if the charge separation between the orders is larger than 3, there is virtually no crosstalk. The system functions without issues when used with charges $l = [-30, -20, -10, 0, 10, 20, 30]$. As seen in Fig. 10, the separation between orders remains constant, and virtually no crosstalk is detected in the system.

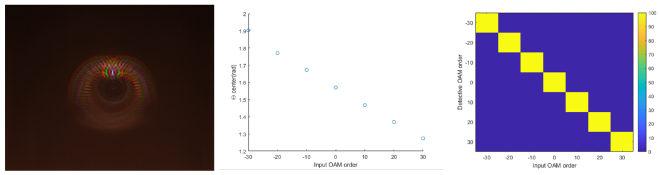

Fig. 10. Experimental output of 6 different input a) TC=[−30,−10,10,30] in red, TC = [−20,20] in green, and TC = 0 in white. b) shows the angular location of the maximum. c) shows the crosstalk.

IV. CONCLUSION

In this paper it has been shown that a free space POV sorter can be fabricated and used with any optical system with minimal modification. The sorter is a hybrid lens that is designed using a superposition of a modified radial lens and a lateral lens. It has been shown that using the combinations of these lenses works well with POV, because of the constant ring size of the POV. The hybrid lens is shown to have many degrees of freedom that can be optimized for a given beam size, and optical system dimensions and constrains. The radial shift of the lens allow for perfect matching between the radial phase and the POV beam width. The introduction of a lateral lens to the radial lens enables for compactness to be archived. The modified constant parameters α and β are demonstrated to control the size, and the angular separation of the sorted beams. The hybrid lens is optimized for 632.8 nm laser and an optical system with a focal length of 175 mm, and an input beam of radius 1 mm and width 0.25 mm. The parameters α and β are optimized to achieve an angular separation of 1°. Simulations are carried out to demonstrate the sorting efficiency of the lens and to evaluate the crosstalk. The lens is fabricated and experimentally tested. The experimental results match the simulations with small deviation that is due to alignment and fabrication error. The crosstalk is also evaluated using both simulation and experiment, and they are in good agreements. The crosstalk is high when using consecutive orders. But, reduced greatly when the input OAM charges are more than 2 orders away from each other.

REFERENCES

[1] L. Allen, M. W. Beijersbergen, R. J. C. Spreeuw, and J. P. Woerdman, "Orbital angular momentum of light and the transformation of Laguerre-Gaussian laser modes," *Phys. Rev. A, Atomic, Mol., Opt. Phys.*, vol. 45, no. 11, pp. 8185–8189, 1992.

[2] A. Trichili, M. A. Cox, B. Perez-Garcia, B. S. Ooi, and M. Alouini, "Theory and practice of orbital angular momentum and beyond," *Digit. Encyclopedia Appl. Phys.*, pp. 1–32, 2021. .

[3] A. S. Ostrovsky, C. Rickenstorff-Parrao, and V. Arrizón, "Generation of the "perfect" optical vortex using a liquid-crystal spatial light modulator," *Opt. Lett.*, vol. 38, no. 4, 2013, Art. no. 534.

[4] J. Garcıa-Garcıa, C. Rickenstorff-Parrao, R. Ramos-Garcıa, V. Arrizón, and A. S. Ostrovsky, "Simple technique for generating the perfect optical vortex," *Opt. Lett.*, vol. 39, no. 18, 2014, Art. no. 5305.

[5] X. Li, Y. Li, X. Zeng, and Y. Han, "Perfect optical vortex array for optical communication based on orbital angular momentum shift keying," *J. Opt.*, vol. 20, no. 12, 2018, Art. no. 125604.

[6] P. Vaity and L. Rusch, "Perfect vortex beam: Fourier transformation of a bessel beam," *Opt. Lett.*, vol. 40, no. 4, 2015, Art. no. 597.

[7] J. Leach, M. J. Padgett, S. M. Barnett, S. Franke-Arnold, and J. Courtial, "Measuring the orbital angular momentum of a single photon," *Phys. Rev. Lett.*, vol. 88, no. 25, 2002, Art. no. 257901.

[8] G. Gibson et al., "Free-space information transfer using light beams carrying orbital angular momentum," *Opt. Exp.*, vol. 12, no. 22, 2004, Art. no. 5448.

[9] G. C. Berkhout, M. P. Lavery, J. Courtial, M. W. Beijersbergen, and M. J. Padgett, "Efficient sorting of orbital angular momentum states of light," *Phys. Rev. Lett.*, vol. 105, no. 15, 2010, Art. no. 153601 .

[10] S. Yu, "Potentials and challenges of using orbital angular momentum communications in optical interconnects," *Opt. Exp.*, vol. 23, no. 3, 2015, Art. no. 3075.

[11] J. Pinnell, V. Rodrıguez-Fajardo, and A. Forbes, "Quantitative orbital angular momentum measurement of perfect vortex beams," *Opt. Lett.*, vol. 44, no. 11, 2019, Art. no. 2736.

[12] A. Volyar, M. Bretsko, Y. Akimova, and Y. Egorov, "Measurement of the vortex spectrum in a vortex-beam array without cuts and gluing of the wavefront," *Opt. Lett.*, vol. 43, no. 22, pp. 5635–5638, 2018.

[13] A. Volyar, M. Bretsko, Y. Akimova, and Y. Egorov, "Measurement of the vortex and orbital angular momentum spectra with a single cylindrical lens," *Appl. Opt.*, vol. 58, no. 21, pp. 5748–5755, 2019.

[14] G. Ruffato, M. Massari, and F. Romanato, "Diffractive optics for combined spatial- and mode-division demultiplexing of optical vortices: Design, fabrication and optical characterization," *Sci. Rep.*, vol. 6, 2016, Art. no. 24760.

[15] H. Huang et al., "Mode division multiplexing using an orbital angular momentum mode sorter and MIMO-DSP over a graded-index few-mode optical fibre," *Sci. Rep.*, vol. 5, 2015, Art. no. 14931.

[16] R. Sahu, S. Chaudhary, K. Khare, M. Bhattacharya, H. Wanare, and A. K. Jha, "Angular lens," *Opt. Exp.*, vol. 26, no. 7, 2018, Art. no. 8709.

[17] J. Zhou, H. Pu, and Q. Wang, "Orbital angular momentum mode sorting based on a hybrid radial-angular hybrid lens," *Opt. Exp.*, vol. 30, no. 6, 2022, Art. no. 9703.

[18] G. Ruffato, "OAM-inspired new optics: The angular metalens," *Light: Sci. Appl.*, vol. 10, no. 1, 2021, Art. no. 96.

[19] Y. Guo et al., "Spin-decoupled metasurface for simultaneous detection of spin and orbital angular momenta via momentum transformation," *Light: Sci. Appl.*, vol. 10, no. 1, 2021, Art. no. 63.

[20] J. Ni et al., "Multidimensional phase singularities in nanophotonics," *Science*, vol. 374, no. 6566, 2021, Art. no. eabj0039.

[21] S. Ijaz, A. S. Rana, Z. Ahmad, M. Zubair, Y. Massoud, and M. Q. Mehmood, "The dawn of metadevices: From contemporary designs to exotic applications," in *Adv. Devices Instrum.*, vol. 20, pp. 1–24, 2022.

[22] A. Leitis, M. L. Tseng, A. John-Herpin, Y. S. Kivshar, and H. Altug, "Wafer-scale functional metasurfaces for mid-infrared photonics and biosensing," *Adv. Mater.*, vol. 33, no. 43, Art. no. 2102232, 2021.

[23] S. Scheiding et al., "Freeform manufacturing of a microoptical lens array on a steep curved substrate by use of a voice coil fast tool servo," *Opt. Exp.*, vol. 19, no. 24, 2011, Art. no. 23938.

[24] M. Born and E. Wolf, *Principles of Optics*. Cambridge, U.K.: Cambridge Univ. Press, 2019.

[25] S. Zheng, R. H. AlIbrahim, O. Alkhazragi, T. Khee Ng, and B. S. Ooi, "Compact, low-cost, and low-crosstalk orbital angular momentum sorter based on binary grating," *Opt. Laser Technol.*, vol. 167, 2023, Art. no. 109744.

[26] J. Arlt, R. Kuhn, and K. Dholakia, "Spatial transformation of Laguerre–Gaussian laser modes," *J. Modern Opt.*, vol. 48, no. 5, pp. 783–787, 2001.

[27] T. Doster and A. T. Watnik, "Machine learning approach to OAM beam demultiplexing via convolutional neural networks," *Appl. Opt.*, vol. 56, no. 12, 2017, Art. no. 3386.